AGU ADVANCING EARTH AND SPACE SCIENCE

Geophysical Research Letters

RESEARCH LETTER
10.1029/2021GL093808

Key Points:

- Greenland ice-core records showed nonsea-salt chlorine increased from the 1940s to 1970s, and decreased leveled off afterward
- Historical simulations by a global model qualitatively capture the observed trends when only considering changes in anthropogenic emissions
- Modeled trends are driven by anthropogenic emissions of sulfur dioxide, nitrogen oxides, and coal combustion-emitted hydrochloric acid

Supporting Information:

Supporting Information may be found in the online version of this article.

Correspondence to:

B. Alexander,
beckya@uw.edu

Citation:

Zhai, S., Wang, X., McConnell, J. R., Geng, L., Cole-Dai, J., Sigl, M., et al. (2021). Anthropogenic impacts on tropospheric reactive chlorine since the preindustrial. *Geophysical Research Letters*, *48*, e2021GL093808. https://doi.org/10.1029/2021GL093808

Received 13 APR 2021
Accepted 19 JUN 2021

Anthropogenic Impacts on Tropospheric Reactive Chlorine Since the Preindustrial

Shuting Zhai[1], Xuan Wang[2], Joseph R. McConnell[3], Lei Geng[4,5], Jihong Cole-Dai[6], Michael Sigl[7], Nathan Chellman[3], Tomás Sherwen[8,9], Ryan Pound[9], Koji Fujita[10], Shohei Hattori[11,12], Jonathan M. Moch[13], Lei Zhu[13,14], Mat Evans[8,9], Michel Legrand[15,16], Pengfei Liu[13,17], Daniel Pasteris[3,18], Yuk-Chun Chan[1], Lee T. Murray[19], and Becky Alexander[1]

[1]Department of Atmospheric Sciences, University of Washington, Seattle, WA, USA, [2]School of Energy and Environment, City University of Hong Kong, Hong Kong SAR, China, [3]Division of Hydrologic Sciences, Desert Research Institute, Reno, NV, USA, [4]School of Earth and Space Sciences, University of Science and Technology of China, Hefei, China, [5]Hefei National Laboratory for Physical Sciences at the Microscale, University of Science and Technology of China, Hefei, China, [6]Department of Chemistry and Biochemistry, South Dakota State University, Brookings, SD, USA, [7]Climate and Environmental Physics, University of Bern, Bern, Switzerland, [8]National Centre for Atmospheric Science, University of York, York, UK, [9]Wolfson Atmospheric Chemistry Laboratories, Department of Chemistry, University of York, York, UK, [10]Graduate School of Environmental Studies, Nagoya University, Nagoya, Japan, [11]Department of Chemical Science and Engineering, School of Materials and Chemical Technology, Tokyo Institute of Technology, Tokyo, Japan, [12]International Center for Isotope Effects Research, Nanjing University, Nanjing, China, [13]School of Engineering and Applied Sciences, Harvard University, Cambridge, MA, USA, [14]Now at School of Environmental Science and Engineering, Southern University of Science and Technology, Shenzhen, China, [15]CNRS, Institut des Géosciences de l'Environnement, Université Grenoble Alpes, Grenoble, France, [16]LISA (Laboratoire Interuniversitaire des Systèmes Atmosphériques), UMR CNRS 7583, Université Paris-Est-Créteil, Université de Paris, Institut Pierre Simon Laplace, Créteil, France, [17]Now at School of Earth and Atmospheric Sciences, Georgia Institute of Technology, Atlanta, GA, USA, [18]Now at McGinley & Associates, Inc., Reno, NV, USA, [19]Department of Earth and Environmental Sciences, University of Rochester, Rochester, NY, USA

Abstract Tropospheric reactive gaseous chlorine (Cl_y) impacts the atmosphere's oxidation capacity with implications for chemically reduced gases such as methane. Here we use Greenland ice-core records of chlorine, sodium, and acidity, and global model simulations to show how tropospheric Cl_y has been impacted by anthropogenic emissions since the 1940s. We show that anthropogenic contribution of nonsea-salt chlorine significantly influenced total chlorine and its trends after the 1940s. The modeled regional 170% Cl_y increase from preindustrial to the 1970s was driven by acid displacement from sea-salt-aerosol, direct emission of hydrochloric acid (HCl) from combustion, and chemical reactions driven by anthropogenic nitrogen oxide (NO_x) emissions. Since the 1970s, the modeled 6% Cl_y decrease was caused mainly by reduced anthropogenic HCl emissions from air pollution mitigation policies. Our findings suggest that anthropogenic emissions of acidic gases and their emission control strategies have substantial impacts on Cl_y with implications for tropospheric oxidants, methane, and mercury.

Plain Language Summary Greenland ice cores preserve information from past atmospheres and provide information on how human activities have changed the composition of the atmosphere. While ice-core chlorine mainly originates from deposited sea-salt particles in the air, we found that emissions from human activities also influence ice-core chlorine. Using six Greenland ice cores and global model simulations, we show that the observed increasing trend in nonsea-salt chlorine during the 1940s–1970s was caused by enhanced human emissions of acidic gases and the resulting chemical reactions involving atmospheric sea-salt particles, and the observed decrease after the 1970s is largely attributed to air pollution control strategies that are widely applied in North America and Europe.

1. Introduction

Chlorine (Cl) in polar ice cores can provide information about past SSA abundance since the main source of ice-core Cl is from the emission and transport of sea-salt-aerosol (SSA). Reactive gaseous chlorine (Cl_y = BrCl + HCl + Cl + ClO + HOCl + $ClNO_3$ + $ClNO_2$ + ClOO + OClO + 2 · Cl_2 + 2 · Cl_2O_2 + ICl)

from anthropogenic emissions, mainly in the form HCl, may also be a significant source of ice-core Cl (Legrand et al., 2002; Pasteris et al., 2014). The impact of anthropogenic emissions on tropospheric reactive chlorine since the preindustrial has not been quantified. Formation of HCl through acid displacement on SSA is thought to be the largest (85%) source of Cl_y in the troposphere (X. Wang et al., 2019), and is influenced by anthropogenic emissions of acid gas precursors such as sulfur dioxide (SO_2) and nitrogen oxides (NO_x = NO + NO_2). HCl is also emitted directly from combustion, mainly coal (Fu et al., 2018; Keene et al., 1999; Kolesar et al., 2018; Y. Liu et al., 2018; McCulloch, Aucott, Benkovitz et al., 1999; McCulloch, Aucott, Graedel et al., 1999). HCl contributes to acid deposition, causing damage to lakes and ecosystems, altering atmospheric acidity (Evans et al., 2011), and leads to severe haze and fog through cocondensation on aerosol (Gunthe et al., 2021). Oxidation of HCl and sea-salt chloride ($_{SSA}Cl^-$) produces more reactive forms of chlorine species, such as the chlorine radical (Cl•) (Bryukov et al., 2006), nitryl chloride ($ClNO_2$) (Finlayson-Pitts et al., 1989; Kercher et al., 2009; Raff et al., 2009), and hypochlorous acid (HOCl) (Watson, 1977). Despite the much lower abundance, these highly reactive chlorine species has potentially large local influence for ozone (Finlayson-Pitts, 2003; Knipping & Dabdub, 2003), nitrogen oxides (Haskins et al., 2019; Thornton et al., 2010), secondary organic aerosol (Choi et al., 2020), methane (Allan et al., 2007; Platt et al., 2004), nonmethane hydrocarbons (Aschmann & Atkinson, 1995; Pszenny et al., 2007), and elemental mercury (Donohoue et al., 2005; Horowitz et al., 2017).

Anthropogenic emissions and acid displacement of HCl can lead to enrichment or depletion of Cl relative to sodium (Na) compared to their ratio in sea water, denoted as Cl_{exc} (Equation 2 in Methods). Legrand et al. (2002) calculated ice-core HCl after removing sea-salt and continental chloride from the measured total chloride, and attributed the increases in alpine ice cores to enhanced coal combustion and waste incineration in western Europe during 1925–1970. Observations show decreasing trends of non-SSA Cl^- deposition over the past 20–30 years in the US (Haskins et al., 2020) and UK (Evans et al., 2011), suggesting that the post-1970s air pollution mitigation policies targeting SO_2 and NO_x emissions have reduced emissions of HCl. At Summit (central Greenland), Legrand et al. (2002) found that Cl_{exc} originates mainly from acid displacement of HCl from SSA, which increased by a factor of 2–3 over the twentieth century due to enhanced aerosol acidity resulting from growing anthropogenic NO_x and SO_2 emissions. Greenland ice-core records of sulfate and nitrate, the main sinks for NO_x and SO_2, show increases beginning in the 1900s, peaking in the 1970s, followed by a rapid decline in sulfate and a more gradual decline in nitrate (Geng et al., 2014), consistent with trends of anthropogenic SO_2 and NO_x emissions from combustion (Smith et al., 2011).

2. Methods

2.1. Ice-Core Records

We present ice-core chlorine, sodium, and acidity records from the six Greenland ice cores (Figure S1**)**. Precise locations and other information are summarized in Table S1, and details on core extraction and dating are described in previous publications (Geng et al., 2014; Iizuka et al., 2018; McConnell et al., 2019; Opel et al., 2013; Spolaor et al., 2016). Measurements of ice-core Na and Cl were using either a continuous flow analysis with an online ion chromatography system (CFA-IC) with an accuracy of 5% at annual resolution (for Summit07) (Geng et al., 2014; Iizuka et al., 2018), or Inductively Coupled Plasma Mass Spectrometry (ICP-MS) (McConnell et al., 2014; Spolaor et al., 2016) with an uncertainty of ±10% (for NEEM, NGT_B19, Tunu, ACT_11d and Summit10). For NEEM, NGT_B19, Tunu, ACT_11d and Summit10 cores, acidity (H^+) was measured directly using a flow-through bubbling chamber method described in Pasteris et al. (2012), with an error less than 5%. For Summit07 ice core, acidity was calculated based on the ion balance, according to Equation 1:

$$\left[H^+\right] = \left[Cl^-\right] + \left[NO_3^-\right] + \left[SO_4^{2-}\right] - \left[Na^+\right] - \left[NH_4^+\right] - \left[K^+\right] - \left[Mg^{2+}\right] - \left[Ca^{2+}\right] \quad (1)$$

with concentrations in units of μeq L^{-1} (Geng et al., 2014). Note that this calculation may underestimate snow acidity because it does not consider organic-acid anions (e.g., formate and acetate), which were measured to be 0.3 ± 0.1 μM at Summit during 1767–1945 (Legrand & Mayewski, 1997).

To separate the contribution of SSA relative to more reactive forms (e.g., HCl) of Cl, we calculated the chlorine excess (Cl_{exc}) relative to what would be expected from SSA alone, which is defined with a sea water Cl/Na mass ratio ($([Cl]/[Na])_{sea\ water}$) of 1.796 (Riley & Tongudai, 1967) (Equation 2):

$$Cl_{exc} = [Cl]_{ice\ core} - \left([Cl]/[Na]\right)_{sea\ water} \times [Na]_{ice\ core} \quad (2)$$

ICP-MS measurements may lead to an underestimate of Cl_{exc} because it measures both the soluble Na and the insoluble Na fraction which may originate from nonsea-salt aerosol (e.g., dust), whereas IC measures the soluble Na and a small fraction of leachable Na from dust.

To analyze the relationship between measured species in the ice cores, we adopt the Passing-Bablok (PB) regression model (Passing & Bablok, 1983). In contrast to the traditional Ordinary Least Squares regression (OLS) which only considers measurement errors on the *y*-axis variable, PB regression assumes both *x*-axis and *y*-axis variables contain measurement errors and is insensitive to outliers (e.g., due to volcanic eruptions). We use the Pearson's correlation coefficient (*r*) to show the relationships between species, and *r* is not affected by the choice of the regression model.

2.2. GEOS-Chem Simulations

To estimate impacts of anthropogenic emissions on tropospheric HCl and reactive chlorine abundances, we use a global 3-D chemical transport model GEOS-Chem (version 11-02d, Text S1) described in Bey et al. (2001) with updates described in the supporting information. The model is driven by MERRA-2 assimilated meteorological observations from the Goddard Earth Observing System (GEOS) (Gelaro et al., 2017). The model simulates detailed HO_x-NO_x-VOC-ozone-halogen-aerosol tropospheric chemistry, which includes SSA (Jaeglé et al., 2011) and tropospheric gas-phase, liquid-phase, and heterogeneous-phase reactive chlorine chemistry (X. Wang et al., 2019), and fully coupled stratospheric chemistry (Eastham et al., 2014).

Model simulations are performed using three emission scenarios: preindustrial (PI, year 1750), peak atmospheric acidity (PA, year 1975), and present day (PD, year 2007), as summarized in Text S1 and Table S2. We run each simulation for 5 years to equilibrate stratosphere-troposphere exchange, and use only the fifth year for analysis. All simulations are conducted at 4° × 5° horizontal resolution and 72 vertical levels up to 0.01 hPa. We use MERRA-2 meteorological fields of the same year (2007) for all three simulations to isolate changes induced by anthropogenic emissions. This configuration will also keep emissions that are dependent on meteorological parameters, such as wind-blown dust, lightning and soil NO_x, biogenic VOCs, and SSA from the open ocean and sea-ice, constant. Only anthropogenic and biomass-burning emissions are allowed to vary between simulations in order to isolate their impacts on tropospheric chlorine.

2.3. Backward Trajectory Analysis

To determine the source regions of Cl_y at the six Greenland ice-core sites, we run backward trajectory analysis using the HYSPLIT model (Hybrid Single-Particle Lagrangian Integrated Trajectory) (Stein et al., 2015). We calculate the cumulative air mass probability for the 5-day backward trajectories, considering the modeled lifetime of acidic gases (e.g., SO_2 and NO_x of about 1 day), accumulation-mode aerosol (up to 6 days) (Alexander et al., 2005), and gas phase HCl (2.5 days), as well as possible seasonal variations in transport. To retrieve the source regions across the ice-core covered time periods, we conduct the backward trajectory analysis for 1959–2010, and present the averaged results. Initial altitudes of air masses are at 10, 500, 1,000 and 1,500 m above ground level (a.g.l.), and the calculation was constrained within 1,500 m a.g.l., which was assumed to be the depth of the mixing layer. Daily precipitation from the reanalysis data sets (ERA-40 and ERA-Interim (Dee et al., 2011; Uppala et al., 2005)) was used for weighting the probability of air masses. Considering the proximity of the two Summit cores, and Tunu and NGT_B19, we only conduct the analysis for four locations: NEEM, Tunu, ACT_11d, and Summit, and chose a region that covers most of the backward trajectory probabilities as the backward trajectory region (TRJ) (Figure S2).

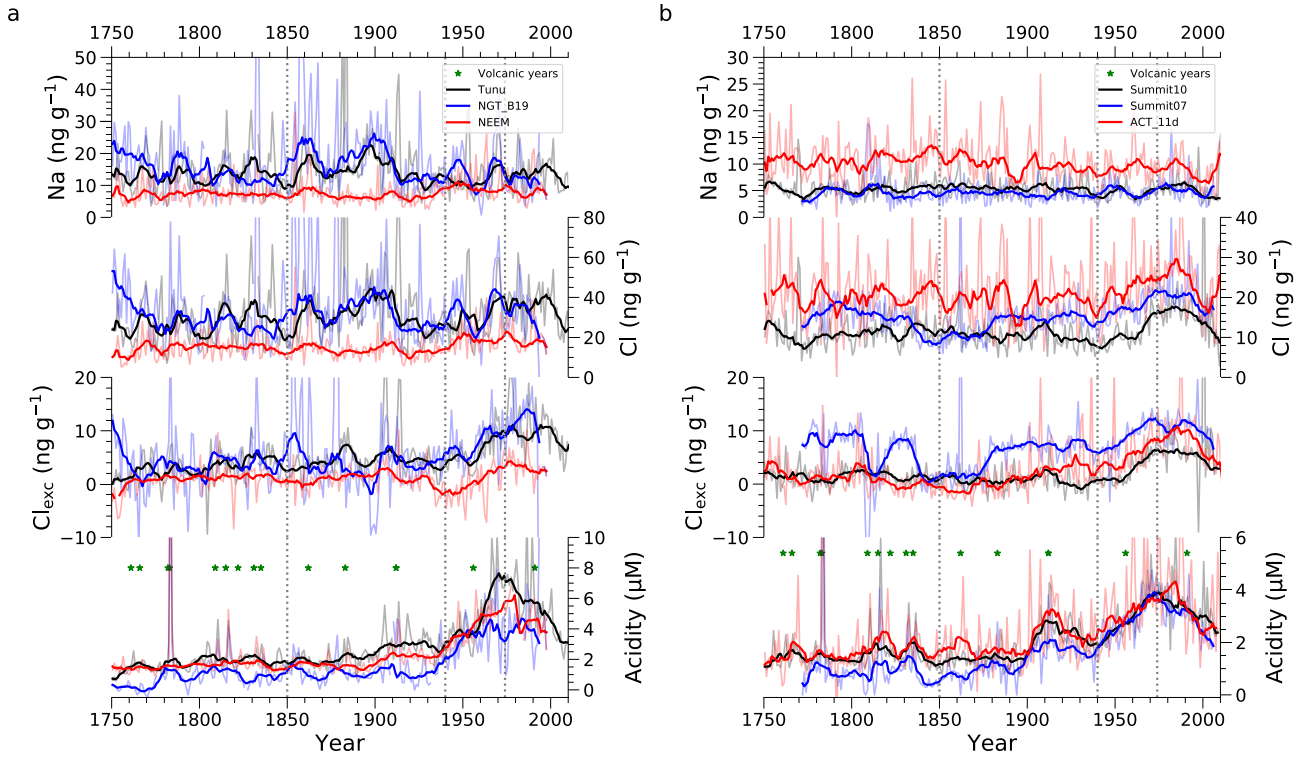

Figure 1. Annual concentrations of Na, Cl, Cl_{exc}, and acidity of the six ice cores in Greenland. (a) Records from higher latitude Greenland ice cores Tunu (black), NGT_B19 (blue), and NEEM (red). (b) Records from lower latitude Greenland ice cores Summit10 (black), Summit07 (blue), and ACT_11d (red). Gray, light blue, and pink lines represent the annual-mean concentrations. Black, blue and red lines represent the 9-years running average concentrations after removing the outliers that are outside of 1.5 × IQR (interquartile range). Green stars mark volcanic eruption years (Text S2). Ion concentrations are reported for Summit07, whereas elemental concentrations are reported for other ice cores. Vertical gray dotted lines mark the years 1850, 1940, and 1975.

3. Results

3.1. Ice-Core Observations

Figure 1 shows annual concentrations of Na, Cl, Cl_{exc}, and acidity from six Greenland ice cores (Figure S1). Positive mean Cl_{exc} values (1.0–5.9 ng g^{-1}) over the reported time periods (1750 or 1776–end of the records) in all records are consistent with negligible loss of HCl from the snowpack after atmospheric deposition where snow accumulation rates are greater than 40 kg m^{-2} yr^{-1} (Röthlisberger, 2003) (Table S1). Cl_{exc} represents a higher fraction of total Cl in lower latitude (medians of 9%–49% over the full records) compared to higher latitude ice cores (medians of 8%–17% over the full records) (Figure S3) likely due to closer proximity to North American (NA) and Western European (WE) anthropogenic source regions, as determined by back trajectory analysis (Figure S2). For all ice cores, Cl_{exc} records show no trends before 1940, followed by a twofold to sevenfold increase until ~1975. After 1975, Cl_{exc} either declined (Summit07, ACT_11d) or leveled off (Summit10, Tunu, NEEM, and NGT_B19). ice-core acidity is similar to Cl_{exc}, with no long-term trends before the 1900s (lower latitude cores) or 1940s (higher latitude cores), an increase from 1940 to 1975, followed by a leveling off or decrease. Acidity trends are consistent with previous Greenland ice-core sulfate records (Geng et al., 2014) and trends in anthropogenic sulfur emissions in NA and WE (Smith et al., 2011).

Figure 2 and Table S3 show relationships between annual ice-core Na and Cl, and between ice-core acidity and Cl_{exc}. Na and Cl were strongly correlated in all ice cores, with a stronger relationship in higher latitude (r = 0.86–0.94) compared to lower latitude (r = 0.49–0.80) cores. Continued strong correlation after the 1940s (Table S3) suggests that SSA was the dominant source of chlorine throughout the records. Correlations between acidity and Cl_{exc} were stronger in post-1940s (r = 0.33–0.72), compared to pre-1940s (r = −0.02–0.43) when acidity was relatively low (Table S3). Lower latitude cores show a higher correlation (r = 0.67–0.72) post-1940s than higher latitude cores (r = 0.33–0.38) due to their closer proximity to anthropogenic source regions.

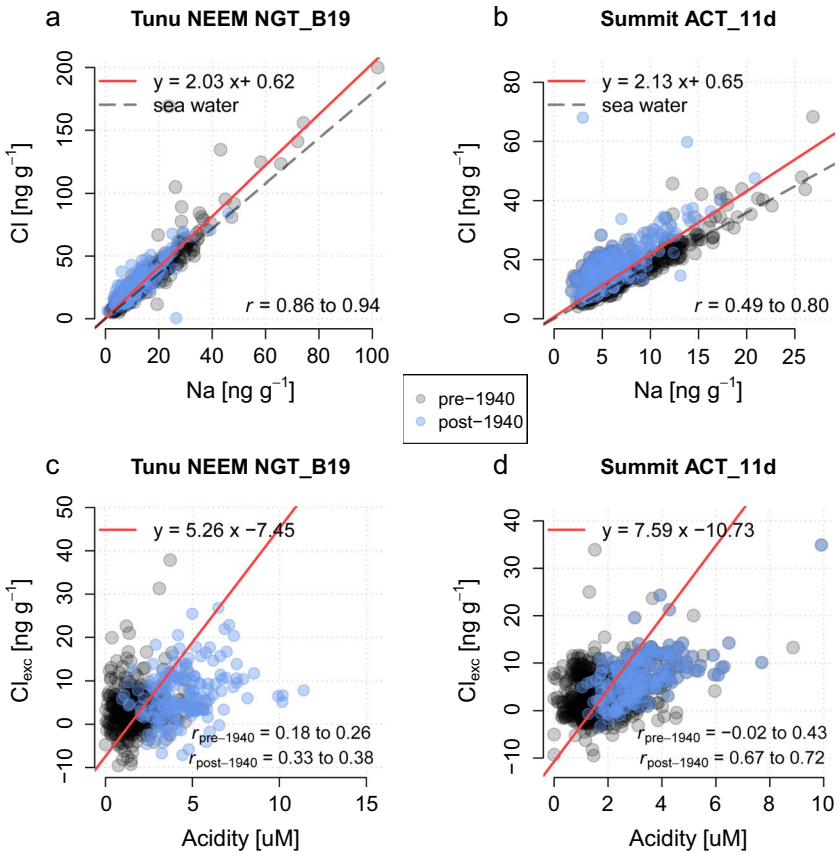

Figure 2. Relationships between annual ice-core (a and b) Na and Cl concentrations, and (c and d) snow acidity and Cl_{exc} from the six Greenland ice-core records. (a and c) Higher latitude cores including Tunu, NEEM, NGT_B19, (b and d) the lower latitude cores including Summit07, Summit10, and ACT_11d. Black circles are the pre-1940 record and blue circles represent post-1940 records. Red lines and the equation show the PB regression for the full record. Dashed black lines show the relationship between Na and Cl in sea water. r, $r_{pre\text{-}1940}$, and $r_{post\text{-}1940}$ represent, respectively, the Pearson's correlation coefficients for the full records, pre-1940 and post-1940 records, and the range of r values is from individual ice cores in the group. Outliers outside the 1.5 × IQR (interquartile range) are removed. All r values are significant with p values lower than 0.05.

3.2. Model-Observation Comparisons

Figure 3 shows the 30°–90°N regional distribution of modeled annual-mean surface Cl_y in PI, PA, and PD, where the model considers past changes in anthropogenic emissions (Methods, and Text S1). Surface Cl_y is shown because most tropospheric Cl_y is confined to lower altitudes (2 km) due to the dominance of direct surface emissions and near-surface chemistry sources (Figure S4). The highest surface Cl_y concentrations in PA and PD are distributed in continental outflow regions where anthropogenic acids encounter $_{SSA}Cl^-$, leading to acid displacement of HCl. The tropospheric burden of Cl_y in the 30°–90°N region increased 132% from PI to PA and 7% from PA to PD. While surface Cl_y increases everywhere in the region from PI to PA and PI to PD, the trend from PA to PD shows spatial variability that is, consistent with regional trends in anthropogenic emissions of SO_2 and NO_x.

The simulated trends in Cl_y in the calculated 5-day back trajectory region (TRJ, green dashed region in Figure 3) are qualitatively consistent with and within the ranges of the observed trends in Greenland ice-core Cl_{exc} (Figure 4a). On average, the modeled Cl_y burden in TRJ increased by 170% from PI to PA, and decreased by 6% from PA to PD. From PI to PA, ice-core Cl_{exc} showed increases ranging from 105% to 631%, with an average increase of 335%. Although modeled average trends from PI to PA lie below the 25th percentile of observations, the modeled increase in Cl_y in continental outflow regions of NA (276%) and WE (203%) lie within the interquartile range (IQR) of the observations, suggesting that trends in chlorine deposition in

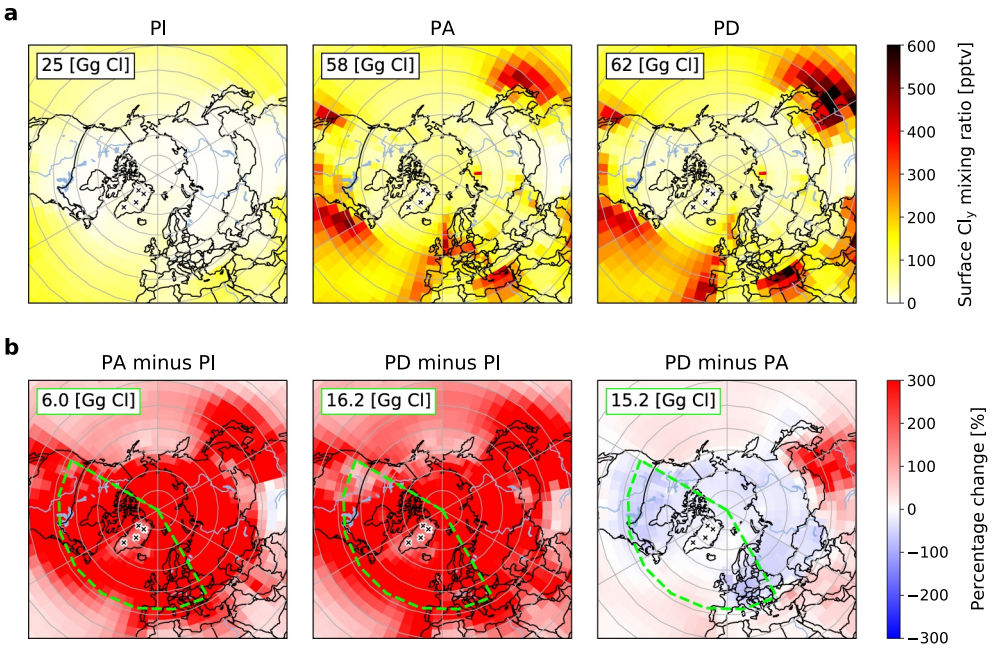

Figure 3. 30°–90°N regional distributions of annual-mean surface mixing ratios of Cl_y in the three-time periods in GEOS-Chem (a), and the percentage difference of Cl_y surface mixing ratio between the three-time periods (b). Gray grid lines show 10° latitude and 60° longitude distance. Black crosses mark the ice-core sites. Dashed green lines show the back trajectory region (TRJ, 120°W–30°E, 42°–90°N) for the six Greenland ice cores based on the 5-day back trajectory analysis. The annual-mean tropospheric Cl_y burdens for 30°–90°N regions are shown on the top-left corners of subplots in (a), and the burdens for the TRJ region are shown similarly in (b).

inland Greenland may be more influenced by these source regions. From PI to PD, the simulated average TRJ Cl_y increased 153%, similar to the median increase (163%) in the observations, and was within the IQR range of the ice-core trends. The average modeled trend (+153%) fell on the lower end of the observed range, but again the simulated trends in NA and WE continental outflow regions (223% and 185%, respectively) showed a more robust comparison with the average change in ice-core Cl_{exc} (253%). From PA to PD, most inland Greenland ice cores showed a decreasing trend in Cl_{exc}, with an average decrease of 20%, and a median decrease of 41%. The magnitude of the average modeled Cl_y trends from PA to PD in the TRJ region (−6%) was smaller than the average of ice-core observations, but the modeled changes in the NA and WE continental source regions (−13%) were more similar to the observations. The range of PA to PD changes in the model (−46% to 19%) fell within the range of the ice-core observations (−114% to 102%). The modeled PI-to-PA (210%) and PA-to-PD (−25%) change in Cl_y at the location of the Col du Dome ice core in the French Alps also was qualitatively consistent with ice-core Cl_{exc} changes (383% from PI to PA, −71% from PA to PD) from Legrand et al. (2002). Model underestimation of the trends may be due in part to uncertainties in anthropogenic HCl emissions (Methods).

3.3. Anthropogenic Impacts on Reactive Gaseous Chlorine

Simulated trends in Cl_y reflect trends in HCl, since >94% of the burden and 99% of deposition is of the form HCl (Figure S5). The dominant source of HCl in all three-time periods is acid displacement of $_{SSA}Cl^-$, contributing 73%, 47%, and 61% to the total source in PI, PA, and PD, respectively (Figure 4b). Chemical reactions that convert Cl* (= Cl_y − HCl) to HCl is the second largest source (20%, 27%, and 26% in PI, PA, and PD, respectively). In PA, the Cl* source is closely followed by direct anthropogenic HCl emissions, which contributes 21% of the total source. Other sources are minor (<10%). The increase in HCl from PI to PA in the TRJ region (mean of 238%) is driven by increases in direct anthropogenic emissions of HCl (35%), acid displacement (29%), and heterogeneous reactions involving Cl* (29%). The 12% decrease in HCl from PA to PD is driven by decreases in the direct anthropogenic source of HCl (71%) and in conversion of Cl* to HCl (16%), and is partly compensated by a continued increase (15%) in acid displacement.

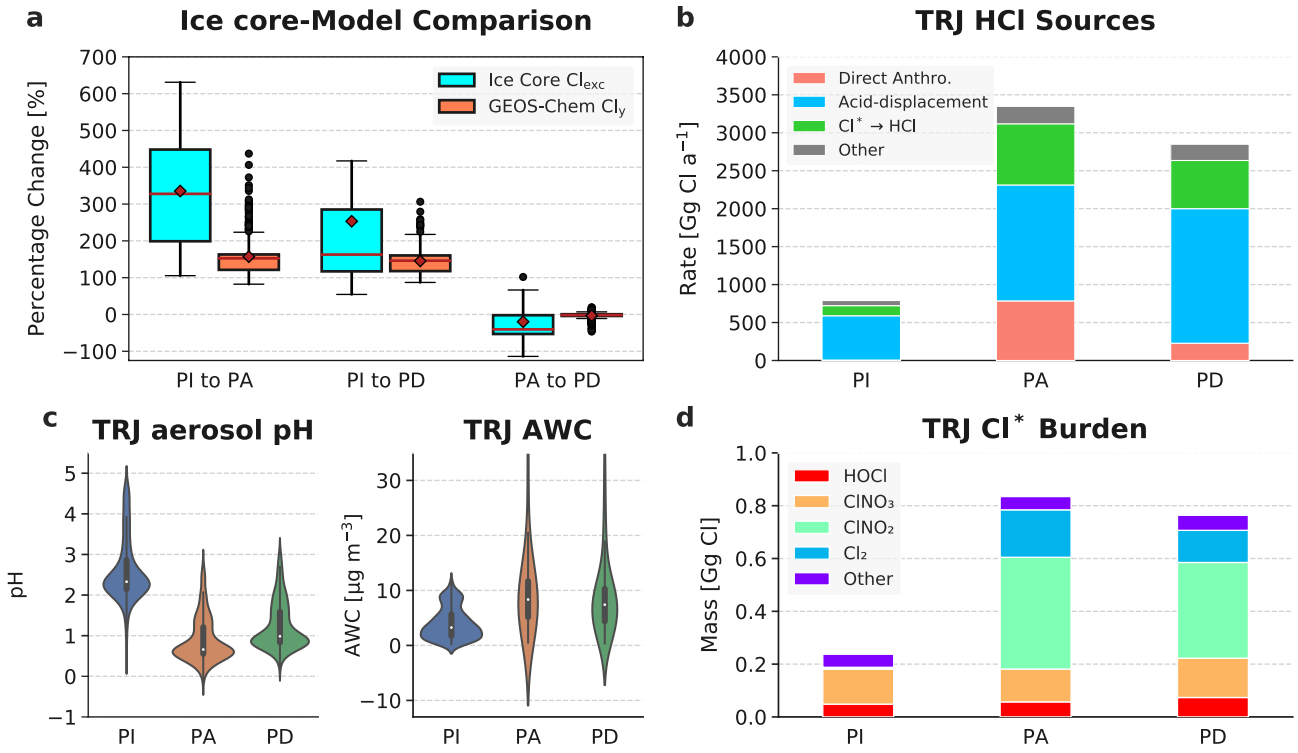

Figure 4. Model-observation comparison of non-SSA chlorine and model interpretation of the trends. (a) Comparison of percentage changes in the Cl_{exc} concentrations from the six Greenland ice cores (blue boxes) and modeled Cl_y burdens in TRJ (orange boxes) between PI, PA, and PD. ice-core statistics are calculated from 1750 to 1760 for PI, 1970–1980 for PA, and the last 10 years of the records for PD. Boxplots show the range of percentage changes, red diamonds mark the mean values and red lines represent the medians. Black dots are model grid boxes outside the range of 1.5 IQR. (b) Modeled HCl sources in TRJ for PI, PA, and PD. "Direct Anthro." refers to direct anthropogenic emissions of HCl. "Cl* → HCl" represents the net conversion of Cl* into HCl. "Other" sources include the stratosphere to troposphere exchange and transport from outside of TRJ (<7%), biomass burning (<2%), and HCl formed from organochlorines (<0.1%). (c) Violin plots for modeled accumulation-mode aerosol pH in TRJ (left panel) and aerosol water content (AWC) in TRJ for PI, PA, and PD. (d) Modeled annual-mean tropospheric Cl* burden (in Gg Cl) in TRJ for PI, PA, and PD. "Other" Cl* species include BrCl, Cl, ClO, ClOO, Cl_2O_2, and ICl.

HCl acid displacement is controlled by thermodynamic equilibrium between gas phase (HCl) and aerosol phase ($_{SSA}Cl^-$). Lower aerosol pH and aerosol water content (AWC) both favor acid displacement of HCl (Haskins et al., 2018), but the relationship is nonlinear. At higher pH in PI, the equilibrium is more sensitive to pH than to AWC. At lower pH in PA and PD, AWC becomes more important (Haskins et al., 2018). From PI to PA, the mean aerosol pH in TRJ decreased 1.7 pH units, resulting in a large increase in HCl displacement despite the increase in AWC (223%) (Figure 4c). From PA to PD, continued increase in HCl displacement is driven by lower AWC in the PD relative to the PA. Although accumulation-mode aerosol pH increases slightly from PA to PD (0.3 pH units), the equilibrium is less sensitive to aerosol pH at the lower pH values during the PA and PD (Haskins et al., 2018) (Figure 4c).

The HCl source from Cl* chemistry originates from reactions between Cl• with hydrocarbons and the in-cloud reaction between dissolved SO_2 and HOCl (Figure S5). Trends in the Cl* source of HCl reflect trends in Cl* abundance. The Cl* burden increased by 252% from PI to PA, and decreased by −9% from PA to PD in TRJ (Figure 4d). Enhanced formation of $ClNO_2$ (395-fold) from heterogeneous reaction of N_2O_5 with particulate chloride, driven by elevated NO_x emissions (Figure S6), dominates the increase in Cl* from PI to PA. The decrease in Cl* from PA to PD is caused by the decrease of $ClNO_2$ (−14%) and Cl_2 (−32%) from PA to PD due to less N_2O_5 in continental outflow regions (Figure S7) driven by a decrease in NO_x emissions (Figure S6), consistent with satellite observations (Kim et al., 2006; Konovalov et al., 2010).

Changes in $ClNO_2$ production from PI to PA and PA to PD drive changes in total Cl* abundance and in all individual Cl* species except Cl• (Figure S5). Opposite to the Cl* trends, Cl• abundance decreased 27% from PI to PA and increased 20% from PA to PD in the TRJ region. These changes are driven by their reactions with alkanes producing HCl (Figure S5 and Table S4). Enhanced emissions of alkanes from transportation

and energy extraction (Hoesly et al., 2018) and increasing methane from PI to PA (Murray, 2016) increased conversion rate of Cl• to HCl, driving the Cl• decrease. From PA to PD, although methane levels continue to increase, anthropogenic emissions of alkanes in NA and WE decrease (Hoesly et al., 2018), resulting in an increase in Cl• from PA to PD. Changes in sink reactions of Cl• are driving the conversion of Cl* to HCl, which shows an increase from PI to PA and a decrease from PA to PD (Figure 4d).

4. Conclusions and Implications

This study investigates total and nonsea-salt chlorine (Cl_{exc}) trends since preindustrial time using six Greenland ice cores and examines the contribution of anthropogenic emissions to these trends using the GEOS-Chem model. Observed trends in inland Greenland ice-core Cl_{exc} are captured by historical model simulations that isolate the impact of changes in anthropogenic emissions while holding meteorology constant. Model results indicate that from PI to PA, the increases in acid displacement of HCl from SSA, direct anthropogenic HCl emissions and enhanced Cl* production were responsible for the increasing trend in Cl_y. From PA to PD, acid displacement continued to increase, but was overcompensated by reduced direct anthropogenic HCl emissions and chemical conversion of Cl* to HCl. Although direct anthropogenic emissions of HCl represent <21% of the total HCl source, it is required to explain the decreasing trends in Cl_{exc} observed in ice cores since PA.

Cycling of Cl_y species can destroy O_3 directly through catalytic cycles, and indirectly through reducing NO_x abundance (X. Wang et al., 2019). Consequently, increases in Cl_y lead to decreases in OH due to reduction in ozone. The implications of Cl_y for ozone, OH and NO_x have been demonstrated previously (X. Wang et al., 2019). This study shows that anthropogenic emissions of HCl, SO_2 and NO_x have had significant impacts on tropospheric Cl_y abundance (up to +170%), which should be considered in the estimation of anthropogenic impacts on changes in tropospheric oxidation capacity.

In addition to the impact of Cl_y on oxidants such as OH, Cl• serves as an oxidant itself (Sherwen et al., 2016; X. Wang et al., 2019), with reactivity 1–2 orders of magnitude higher than OH in oxidizing alkanes (Atkinson et al., 2006; Finlayson-Pitts & Pitts, 1999; Ji et al., 2013; Xie et al., 2017; Young et al., 2014). Although a minor sink for methane, reaction with Cl• has a large impact on methane's isotopic composition (Strode et al., 2020), which is used to constrain the methane budget in present and past climates (Allan et al., 2001, 2007; Bock et al., 2017; Strode et al., 2020; Whiticar & Schaefer, 2007). Our model simulations suggest that anthropogenic emissions alone have changed the global Cl• abundance by up to −16% since preindustrial times, which will influence the isotopic composition of methane and potentially the isotope-based interpretation of the methane budget.

Acknowledgments
Becky Alexander, Shuting Zhai, and Yuk-Chun Chan acknowledge support from U.S. National Science Foundation (NSF) grants 1702266, 1644998, and 1904128. Shohei Hattori acknowledges support from MEXT/JSPS KAKENHI Grants JP16H05884 and JP20H04305. For Summit07, ice-core collection, analysis, and interpretation were supported by NSF Grants 0612461 and 0839066 to Jihong Cole-Dai. Lei Geng acknowledges support from the National Natural Science Foundation of China (Awards: 41822605). For all other ice cores, Joseph R. McConnell acknowledges support from NSF grants 0909541, 1023672, 1204176, and 1702830. The authors also thank the Danish-led North Greenland Eemian Ice Drilling (NEEM) consortium, the Alfred Wegener Institute, the U.S. Ice Drilling Program, as well as staff and students of the DRI ice core laboratory including O. Maselli, and L. Layman. Shuting Zhai acknowledges fruitful discussions with L. Jaeglé, H. Horowitz, J. Huang, V. Shah, J. Shao, and Q. Chen.

Data Availability Statement

ice-core data for this research is available at the Arctic Data Center via https://doi.org/10.18739/A2X-S5JJ1N with Creative Commons Attribution. GEOS-Chem is open software and available on https://doi.org/10.5281/zenodo.5047976. GEOS-Chem historical simulation output is archived in the University of Washington ResearchWorks repository via http://hdl.handle.net/1773/46969.

References

Alexander, B., Park, R. J., Jacob, D. J., Li, Q. B., Yantosca, R. M., Savarino, J., et al. (2005). Sulphate formation in sea-salt aerosols: Constraints from oxygen isotopes. *Journal of Geophysical Research*, *110*, D10307. https://doi.org/10.1029/2004jd005659

Allan, W., Lowe, D. C., & Cainey, J. M. (2001). Active chlorine in the remote marine boundary layer: Modeling anomalous measurements of $\delta^{13}C$ in methane. *Geophysical Research Letters*, *28*(17), 3239–3242. https://doi.org/10.1029/2001gl013064

Allan, W., Struthers, H., & Lowe, D. C. (2007). Methane carbon isotope effects caused by atomic chlorine in the marine boundary layer: Global model results compared with Southern Hemisphere measurements. *Journal of Geophysical Research*, *112*, D04306. https://doi.org/10.1029/2006JD007369

Aschmann, S. M., & Atkinson, R. (1995). Rate constants for the gas-phase reactions of alkanes with Cl atoms at 296 ± 2 K. *International Journal of Chemical Kinetics*, *27*(6), 613–622. https://doi.org/10.1002/kin.550270611

Atkinson, R., Baulch, D. L., Cox, R. A., Crowley, J. N., Hampson, R. F., Hynes, R. G., et al. (2006). Evaluated kinetic and photochemical data for atmospheric chemistry: Volume II--gas phase reactions of organic species. *Atmospheric Chemistry and Physics*, *6*(11), 3625–4055. https://doi.org/10.5194/acp-6-3625-2006

Bey, I., Jacob, D. J., Yantosca, R. M., Logan, J. A., Field, B. D., Fiore, A. M., et al. (2001). Global modeling of tropospheric chemistry with assimilated meteorology: Model description and evaluation. *Journal of Geophysical Research*, *106*(D19), 23073–23095. https://doi.org/10.1029/2001JD000807

Bock, M., Schmitt, J., Beck, J., Seth, B., Chappellaz, J., & Fischer, H. (2017). Glacial/interglacial wetland, biomass burning, and geologic methane emissions constrained by dual stable isotopic CH_4 ice core records. *Proceedings of the National Academy of Sciences of the United States of America*, *114*(29), E5778–E5786. https://doi.org/10.1073/pnas.1613883114

Bryukov, M. G., Dellinger, B., & Knyazev, V. D. (2006). Kinetics of the gas-phase reaction of OH with HCl. *The Journal of Physical Chemistry A*, *110*(3), 936–943. https://doi.org/10.1021/jp053615x

Choi, M. S., Qiu, X., Zhang, J., Wang, S., Li, X., Sun, Y., et al. (2020). Study of secondary organic aerosol formation from chlorine radical-initiated oxidation of volatile organic compounds in a polluted atmosphere using a 3D chemical transport model. *Environmental Science & Technology*, *54*(21), 13409–13418. https://doi.org/10.1021/acs.est.0c02958

Dee, D. P., Uppala, S. M., Simmons, A. J., Berrisford, P., Poli, P., Kobayashi, S., et al. (2011). The ERA-Interim reanalysis: Configuration and performance of the data assimilation system. *Quarterly Journal of the Royal Meteorological Society*, *137*(656), 553–597. https://doi.org/10.1002/qj.828

Donohoue, D. L., Bauer, D., & Hynes, A. J. (2005). Temperature and pressure dependent rate coefficients for the reaction of Hg with Cl and the reaction of Cl with Cl: A pulsed laser photolysis-pulsed laser induced fluorescence study. *The Journal of Physical Chemistry A*, *109*(34), 7732–7741. https://doi.org/10.1021/jp051354l

Eastham, S. D., Weisenstein, D. K., & Barrett, S. R. H. (2014). Development and evaluation of the unified tropospheric-stratospheric chemistry extension (UCX) for the global chemistry-transport model GEOS-Chem. *Atmospheric Environment*, *89*, 52–63. https://doi.org/10.1016/j.atmosenv.2014.02.001

Evans, C. D., Monteith, D. T., Fowler, D., Cape, J. N., & Brayshaw, S. (2011). Hydrochloric acid: An overlooked driver of environmental change. *Environmental Science & Technology*, *45*(5), 1887–1894. https://doi.org/10.1021/es103574u

Finlayson-Pitts, B. J. (2003). The tropospheric chemistry of sea salt: A molecular-level view of the chemistry of NaCl and NaBr. *Chemical Reviews*, *103*(12), 4801–4822. https://doi.org/10.1021/cr020653t

Finlayson-Pitts, B. J., Ezell, M. J., & Pitts, J. N. (1989). Formation of chemically active chlorine compounds by reactions of atmospheric NaCl particles with gaseous N_2O_5 and $ClONO_2$. *Nature*, *337*, 241–244. https://doi.org/10.1038/337241a0

Finlayson-Pitts, B. J., & Pitts, J. N., Jr. (1999). *Chemistry of the upper and lower atmosphere: Theory, experiments, and applications*. Elsevier. Retrieved from https://play.google.com/store/books/details?id=mRoJUB5fxRwC

Fu, X., Wang, T., Wang, S., Zhang, L., Cai, S., Xing, J., & Hao, J. (2018). Anthropogenic emissions of hydrogen chloride and fine particulate chloride in China. *Environmental Science & Technology*, *52*(3), 1644–1654. https://doi.org/10.1021/acs.est.7b05030

Gelaro, R., McCarty, W., Suárez, M. J., Todling, R., Molod, A., Takacs, L., et al. (2017). The Modern-Era Retrospective Analysis for Research and Applications, Version 2 (MERRA-2). *Journal of Climate*, *30*(13), 5419–5454. https://doi.org/10.1175/JCLI-D-16-0758.1

Geng, L., Alexander, B., Cole-Dai, J., Steig, E. J., Savarino, J., Sofen, E. D., & Schauer, A. J. (2014). Nitrogen isotopes in ice core nitrate linked to anthropogenic atmospheric acidity change. *Proceedings of the National Academy of Sciences of the United States of America*, *111*(16), 5808–5812. https://doi.org/10.1073/pnas.1319441111

Gunthe, S. S., Liu, P., Panda, U., Raj, S. S., Sharma, A., Darbyshire, E., et al. (2021). Enhanced aerosol particle growth sustained by high continental chlorine emission in India. *Nature Geoscience*, *14*, 77–84. https://doi.org/10.1038/s41561-020-00677-x

Haskins, J. D., Jaeglé, L., Shah, V., & Lee, B. H. (2018). Wintertime gas-particle partitioning and speciation of inorganic chlorine in the lower troposphere over the Northeast United States and Coastal Ocean. *Journal of Geophysical Research: Atmospheres*, *123*, 12897–12916. https://doi.org/10.1029/2018jd028786

Haskins, J. D., Jaeglé, L., & Thornton, J. A. (2020). Significant decrease in wet deposition of anthropogenic chloride across the Eastern United States, 1998–2018. *Geophysical Research Letters*, *47*, e2020GL090195. https://doi.org/10.1029/2020gl090195

Haskins, J. D., Lee, B. H., Lopez-Hilifiker, F. D., Peng, Q., Jaeglé, L., Reeves, J. M., et al. (2019). Observational constraints on the formation of Cl_2 from the reactive uptake of $ClNO_2$ on aerosols in the polluted marine boundary layer. *Journal of Geophysical Research: Atmospheres*, *124*, 8851–8869. https://doi.org/10.1029/2019JD030627

Hoesly, R. M., Smith, S. J., Feng, L., Klimont, Z., Janssens-Maenhout, G., Pitkanen, T., et al. (2018). Historical (1750–2014) anthropogenic emissions of reactive gases and aerosols from the Community Emissions Data System (CEDS). *Geoscientific Model Development*, *11*(1), 369–408. https://doi.org/10.5194/gmd-11-369-2018

Horowitz, H. M., Jacob, D. J., Zhang, Y., Dibble, T. S., Slemr, F., Amos, H. M., et al. (2017). A new mechanism for atmospheric mercury redox chemistry: Implications for the global mercury budget. *Atmospheric Chemistry and Physics*, *17*(10), 6353–6371. https://doi.org/10.5194/acp-17-6353-2017

Iizuka, Y., Uemura, R., Fujita, K., Hattori, S., Seki, O., Miyamoto, C., et al. (2018). A 60 year record of atmospheric aerosol depositions preserved in a high-accumulation dome ice core, Southeast Greenland. *Journal of Geophysical Research: Atmospheres*, *123*, 574–589. https://doi.org/10.1002/2017JD026733

Jaeglé, L., Quinn, P. K., Bates, T. S., Alexander, B., & Lin, J.-T. (2011). Global distribution of sea salt aerosols: New constraints from in situ and remote sensing observations. *Atmospheric Chemistry and Physics*, *11*(7), 3137–3157. https://doi.org/10.5194/acp-11-3137-2011

Ji, Y. M., Wang, H. H., Gao, Y. P., Li, G. Y., & An, T. C. (2013). A theoretical model on the formation mechanism and kinetics of highly toxic air pollutants from halogenated formaldehydes reacted with halogen atoms. *Atmospheric Chemistry and Physics Discussions*, *13*(7), 18205–18231. https://doi.org/10.5194/acpd-13-18205-2013

Keene, W. C., Khalil, M. A. K., Erickson, D. J., III, McCulloch, A., Graedel, T. E., Lobert, J. M., et al. (1999). Composite global emissions of reactive chlorine from anthropogenic and natural sources: Reactive Chlorine Emissions Inventory. *Journal of Geophysical Research*, *104*(D7), 8429–8440. https://doi.org/10.1029/1998JD100084

Kercher, J. P., Riedel, T. P., & Thornton, J. A. (2009). Chlorine activation by N_2O_5: Simultaneous, in situ detection of $ClNO_2$ and N_2O_5 by chemical ionization mass spectrometry. *Atmospheric Measurement Techniques*, *2*, 193–204.

Kim, S.-W., Heckel, A., McKeen, S. A., Frost, G. J., Hsie, E.-Y., Trainer, M. K., et al. (2006). Satellite-observed U.S. power plant NO_x emission reductions and their impact on air quality. *Geophysical Research Letters*, *33*, L22812. https://doi.org/10.1029/2006GL027749

Knipping, E. M., & Dabdub, D. (2003). Impact of chlorine emissions from sea-salt aerosol on coastal urban ozone. *Environmental Science & Technology*, *37*(2), 275–284. https://doi.org/10.1021/es025793z

Kolesar, K. R., Mattson, C. N., Peterson, P. K., May, N. W., Prendergast, R. K., & Pratt, K. A. (2018). Increases in wintertime PM2.5 sodium and chloride linked to snowfall and road salt application. *Atmospheric Environment*, *177*, 195–202. https://doi.org/10.1016/j.atmosenv.2018.01.008

Konovalov, I. B., Beekmann, M., Richter, A., Burrows, J. P., & Hilboll, A. (2010). Multi-annual changes of NOx emissions in megacity regions: Nonlinear trend analysis of satellite measurement based estimates. *Atmospheric Chemistry and Physics*, *10*(17), 8481–8498. https://doi.org/10.5194/acp-10-8481-2010

Legrand, M., & Mayewski, P. (1997). Glaciochemistry of polar ice cores: A review. *Reviews of Geophysics*, *35*(3), 219–243. https://doi.org/10.1029/96RG03527

Legrand, M., Preunkert, S., Wagenbach, D., & Fischer, H. (2002). Seasonally resolved Alpine and Greenland ice core records of anthropogenic HCl emissions over the 20th century. *Journal of Geophysical Research*, *107*(D12), ACH 4-1–ACH 4-14. https://doi.org/10.1029/2001jd001165

Liu, Y., Fan, Q., Chen, X., Zhao, J., Ling, Z., Hong, Y., et al. (2018). Modeling the impact of chlorine emissions from coal combustion and prescribed waste incineration on tropospheric ozone formation in China. *Atmospheric Chemistry and Physics*, *18*(4), 2709–2724. https://doi.org/10.5194/acp-18-2709-2018

McConnell, J. R., Chellman, N. J., Wilson, A. I., Stohl, A., Arienzo, M. M., Eckhardt, S., et al. (2019). Pervasive Arctic lead pollution suggests substantial growth in medieval silver production modulated by plague, climate, and conflict. *Proceedings of the National Academy of Sciences of the United States of America*, *116*(30), 14910–14915. https://doi.org/10.1073/pnas.1904515116

McConnell, J. R., Maselli, O. J., Sigl, M., Vallelonga, P., Neumann, T., Anschütz, H., et al. (2014). Antarctic-wide array of high-resolution ice core records reveals pervasive lead pollution began in 1889 and persists today. *Scientific Reports*, *4*, 5848. https://doi.org/10.1038/srep05848

McCulloch, A., Aucott, M. L., Benkovitz, C. M., Graedel, T. E., Kleiman, G., Midgley, P. M., & Li, Y.-F. (1999). Global emissions of hydrogen chloride and chloromethane from coal combustion, incineration and industrial activities: Reactive Chlorine Emissions Inventory. *Journal of Geophysical Research*, *104*(D7), 8391–8403. https://doi.org/10.1029/1999JD900025

McCulloch, A., Aucott, M. L., Graedel, T. E., Kleiman, G., Midgley, P. M., & Li, Y.-F. (1999). Industrial emissions of trichloroethene, tetrachloroethene, and dichloromethane: Reactive chlorine emissions inventory. *Journal of Geophysical Research*, *104*(D7), 8417–8427. https://doi.org/10.1029/1999jd900011

Murray, L. T. (2016). Lightning NO_x and impacts on air quality. *Current Pollution Reports*, *2*(2), 115–133. https://doi.org/10.1007/s40726-016-0031-7

Opel, T., Fritzsche, D., & Meyer, H. (2013). Eurasian Arctic climate over the past millennium as recorded in the Akademii Nauk ice core (Severnaya Zemlya). *Climate of the Past*, *9*(5), 2379–2389. https://doi.org/10.5194/cp-9-2379-2013

Passing, H., & Bablok, W. (1983). A new biometrical procedure for testing the equality of measurements from two different analytical methods. Application of linear regression procedures for method comparison studies in clinical chemistry, Part I. Journal of Clinical Chemistry and Clinical Biochemistry. *Zeitschrift Fur Klinische Chemie Und Klinische Biochemie*, *21*(11), 709–720. https://doi.org/10.1515/cclm.1983.21.11.709

Pasteris, D., McConnell, J. R., Edwards, R., Isaksson, E., & Albert, M. R. (2014). Acidity decline in Antarctic ice cores during the Little Ice Age linked to changes in atmospheric nitrate and sea salt concentrations. *Journal of Geophysical Research: Atmospheres*, *119*, 5640–5652. https://doi.org/10.1002/2013JD020377

Pasteris, D. R., McConnell, J. R., & Edwards, R. (2012). High-resolution, continuous method for measurement of acidity in ice cores. *Environmental Science & Technology*, *46*(3), 1659–1666. https://doi.org/10.1021/es202668n

Platt, U., Allan, W., & Lowe, D. (2004). Hemispheric average Cl atom concentration from $^{13}C/^{12}C$ ratios in atmospheric methane. *Atmospheric Chemistry and Physics*, *4*, 2393–2399. https://doi.org/10.5194/acp-4-2393-2004

Pszenny, A. A. P., Fischer, E. V., Russo, R. S., Sive, B. C., & Varner, R. K. (2007). Estimates of Cl atom concentrations and hydrocarbon kinetic reactivity in surface air at Appledore Island, Maine (USA), during International Consortium for Atmospheric Research on Transport and Transformation/Chemistry of Halogens at the Isles of Shoals. *Journal of Geophysical Research*, *112*, D10S13. https://doi.org/10.1029/2006JD007725

Raff, J. D., Njegic, B., Chang, W. L., Gordon, M. S., Dabdub, D., Gerber, R. B., & Finlayson-Pitts, B. J. (2009). Chlorine activation indoors and outdoors via surface-mediated reactions of nitrogen oxides with hydrogen chloride. *Proceedings of the National Academy of Sciences of the United States of America*, *106*(33), 13647–13654. https://doi.org/10.1073/pnas.0904195106

Riley, J. P., & Tongudai, M. (1967). The major cation/chlorinity ratios in sea water. *Chemical Geology*, *2*, 263–269. https://doi.org/10.1016/0009-2541(67)90026-5

Sherwen, T., Schmidt, J. A., Evans, M. J., Carpenter, L. J., Großmann, K., Eastham, S. D., et al. (2016). Global impacts of tropospheric halogens (Cl, Br, I) on oxidants and composition in GEOS-Chem. *Atmospheric Chemistry and Physics*, *16*(18), 12239–12271. https://doi.org/10.5194/acp-16-12239-2016

Smith, S. J., van Aardenne, J., Klimont, Z., Andres, R. J., Volke, A., & Delgado Arias, S. (2011). Anthropogenic sulfur dioxide emissions: 1850–2005. *Atmospheric Chemistry and Physics*, *11*(3), 1101–1116. https://doi.org/10.5194/acp-11-1101-2011

Spolaor, A., Opel, T., McConnell, J. R., Maselli, O. J., Spreen, G., Varin, C., et al. (2016). Halogen-based reconstruction of Russian Arctic sea ice area from the Akademii Nauk ice core (Severnaya Zemlya). *The Cryosphere*, *10*(1), 245–256. https://doi.org/10.5194/tc-10-245-2016

Stein, A. F., Draxler, R. R., Rolph, G. D., Stunder, B. J. B., Cohen, M. D., & Ngan, F. (2015). NOAA's HYSPLIT atmospheric transport and dispersion modeling system. *Bulletin of the American Meteorological Society*, *96*(12), 2059–2077. https://doi.org/10.1175/bams-d-14-00110.1

Strode, S. A., Wang, J. S., Manyin, M., Duncan, B., Hossaini, R., Keller, C. A., et al. (2020). Strong sensitivity of the isotopic composition of methane to the plausible range of tropospheric chlorine [Data Set]. *Atmospheric Chemistry and Physics*, *20*, 8405–8419. https://doi.org/10.5194/acp-20-8405-2020

Thornton, J. A., Kercher, J. P., Riedel, T. P., Wagner, N. L., Cozic, J., Holloway, J. S., et al. (2010). A large atomic chlorine source inferred from mid-continental reactive nitrogen chemistry. *Nature*, *464*(7286), 271–274. https://doi.org/10.1038/nature08905

Uppala, S. M., KÅllberg, P. W., Simmons, A. J., Andrae, U., Bechtold, V. D. C., Fiorino, M., et al. (2005). The ERA-40 re-analysis. *Quarterly Journal of the Royal Meteorological Society*, *131*(612), 2961–3012. https://doi.org/10.1256/qj.04.176

Wang, X., Jacob, D. J., Eastham, S. D., Sulprizio, M. P., Zhu, L., Chen, Q., et al. (2019). The role of chlorine in global tropospheric chemistry. *Atmospheric Chemistry and Physics*, *19*(6), 3981–4003. https://doi.org/10.5194/acp-19-3981-2019

Watson, R. T. (1977). Rate constants for reactions of ClO_x of atmospheric interest. *Journal of Physical and Chemical Reference Data*, *6*(3), 871–918. https://doi.org/10.1063/1.555558

Whiticar, M., & Schaefer, H. (2007). Constraining past global tropospheric methane budgets with carbon and hydrogen isotope ratios in ice. *Philosophical Transactions. Series A, Mathematical, Physical, and Engineering Sciences*, *365*(1856), 1793–1828. https://doi.org/10.1098/rsta.2007.2048

Xie, H.-B., Ma, F., Yu, Q., He, N., & Chen, J. (2017). Computational study of the reactions of chlorine radicals with atmospheric organic compounds featuring NH_x-π-Bond (x = 1, 2) structures. *The Journal of Physical Chemistry A*, *121*(8), 1657–1665. https://doi.org/10.1021/acs.jpca.6b11418

Young, C. J., Washenfelder, R. A., Edwards, P. M., Parrish, D. D., Gilman, J. B., Kuster, W. C., et al. (2014). Chlorine as a primary radical: Evaluation of methods to understand its role in initiation of oxidative cycles. *Atmospheric Chemistry and Physics*, *14*(7), 3427–3440. https://doi.org/10.5194/acp-14-3427-2014

References From the Supporting Information

Amos, H. M., Jacob, D. J., Holmes, C. D., Fisher, J. A., Wang, Q., Yantosca, R. M., et al. (2012). Gas-particle partitioning of atmospheric Hg(II) and its effect on global mercury deposition. *Atmospheric Chemistry and Physics*, *12*(1), 591–603. https://doi.org/10.5194/acp-12-591-2012

Chen, Q., Schmidt, J. A., Shah, V., Jaeglé, L., Sherwen, T., & Alexander, B. (2017). Sulphate production by reactive bromine: Implications for the global sulfur and reactive bromine budgets: Sulfur-Halogen Interactions. *Geophysical Research Letters*, *44*(13), 7069–7078. https://doi.org/10.1002/2017GL073812

Cole-Dai, J., Ferris, D. G., Lanciki, A. L., Savarino, J., Thiemens, M. H., & McConnell, J. R. (2013). Two likely stratospheric volcanic eruptions in the 1450s C.E. found in a bipolar, subannually dated 800 year ice core record: TWO VOLCANIC ERUPTIONS IN THE 1450s. *Journal of Geophysical Research: Atmospheres*, *118*(14), 7459–7466. https://doi.org/10.1002/jgrd.50587

Custard, K. D., Raso, A. R. W., Shepson, P. B., Staebler, R. M., & Pratt, K. A. (2017). Production and Release of Molecular Bromine and Chlorine from the Arctic Coastal Snowpack. *ACS Earth and Space Chemistry*, *1*(3), 142–151. https://doi.org/10.1021/acsearthspacechem.7b00014

Dlugokencky, E. J. (2016). *Atmospheric methane dry air mole fractions (1983–2015) and atmospheric carbon dioxide dry air mole fractions (1968–2015) from the NOAA ESRL carbon cycle cooperative global air sampling network, original data files.* Retrieved from https://epic.awi.de/id/eprint/44810/

Fisher, J. A., Jacob, D. J., Wang, Q., Bahreini, R., Carouge, C. C., Cubison, M. J., et al. (2011). Sources, distribution, and acidity of sulphate–ammonium aerosol in the Arctic in winter–spring. *Atmospheric Environment*, *45*(39), 7301–7318. https://doi.org/10.1016/j.atmosenv.2011.08.030

Fountoukis, C., & Nenes, A. (2007). ISORROPIA II: A computationally efficient thermodynamic equilibrium model for K–Ca–Mg–NH–Na–SO–NO–Cl–HO aerosols. *Atmospheric Chemistry and Physics*, *7*, 4639–4659. https://doi.org/10.5194/acp-7-4639-2007

Halfacre, J. W., Shepson, P. B., & Pratt, K. A. (2019). pH-dependent production of molecular chlorine, bromine, and iodine from frozen saline surfaces. *Atmospheric Chemistry and Physics*, *19*(7), 4917–4931. https://doi.org/10.5194/acp-19-4917-2019

Holmes, C. D., Bertram, T. H., Confer, K. L., Graham, K. A., Ronan, A. C., Wirks, C. K., & Shah, V. (2019). The role of clouds in the tropospheric NO_x cycle: A new modeling approach for cloud chemistry and its global implications. *Geophysical Research Letters*, *46*, 4980–4990. https://doi.org/10.1029/2019GL081990

Huang, J., & Jaeglé, L. (2017). Wintertime enhancements of sea salt aerosol in polar regions consistent with a sea ice source from blowing snow. *Atmospheric Chemistry and Physics*, *17*(5), 3699–3712. https://doi.org/10.5194/acp-17-3699-2017

Jacob, D. J., Waldman, J. M., Munger, J. W., & Hoffmann, M. R. (1985). Chemical composition of fogwater collected along the California coast. *Environmental Science & Technology*, *19*(8), 730–736. https://doi.org/10.1021/es00138a013

Lee, B. H., Lopez-Hilfiker, F. D., Schroder, J. C., Campuzano-Jost, P., Jimenez, J. L., McDuffie, E. E., et al. (2018). Airborne observations of reactive inorganic chlorine and bromine species in the exhaust of coal-fired power plants. *Journal of Geophysical Research: Atmospheres*, *123*, 11225–11237. https://doi.org/10.1029/2018JD029284

Li, M., Zhang, Q., Streets, D. G., He, K. B., Cheng, Y. F., Emmons, L. K., et al. (2014). Mapping Asian anthropogenic emissions of non-methane volatile organic compounds to multiple chemical mechanisms. *Atmospheric Chemistry and Physics*, *14*(11), 5617–5638. https://doi.org/10.5194/acp-14-5617-2014

Liang, Q., Stolarski, R. S., Kawa, S. R., Nielsen, J. E., Douglass, A. R., Rodriguez, J. M., et al. (2010). Finding the missing stratospheric Bry: A global modeling study of $CHBr_3$ and CH_2Br_2. *Atmospheric Chemistry and Physics*, *10*(5), 2269–2286. https://doi.org/10.5194/acp-10-2269-2010

Liao, J., Huey, L. G., Liu, Z., Tanner, D. J., Cantrell, C. A., Orlando, J. J., et al. (2014). High levels of molecular chlorine in the Arctic atmosphere. *Nature Geoscience*, *7*(2), 91–94. https://doi.org/10.1038/ngeo2046

Liu, H., Jacob, D. J., Bey, I., & Yantosca, R. M. (2001). Constraints from ^{210}Pb and ^{7}Be on wet deposition and transport in a global three-dimensional chemical tracer model driven by assimilated meteorological fields. *Journal of Geophysical Research*, *106*(D11), 12109–12128. https://doi.org/10.1029/2000jd900839

Liu, T., & Abbatt, J. P. D. (2020). An experimental assessment of the importance of S(IV) oxidation by hypohalous acids in the marine atmosphere. *Geophysical Research Letters*, *47*, D23202. https://doi.org/10.1029/2019GL086465

Marais, E. A., & Wiedinmyer, C. (2016). Air quality impact of diffuse and inefficient combustion emissions in Africa (DICE-Africa). *Environmental Science & Technology*, *50*(19), 10739–10745. https://doi.org/10.1021/acs.est.6b02602

Maselli, O. J., Chellman, N. J., Grieman, M., Layman, L., McConnell, J. R., Pasteris, D., et al. (2017). Sea ice and pollution-modulated changes in Greenland ice core methanesulfonate and bromine. *Climate of the Past*, *13*(1), 39–59. https://doi.org/10.5194/cp-13-39-2017

Meinshausen, M., Vogel, E., Nauels, A., Lorbacher, K., Meinshausen, N., Etheridge, D. M., et al. (2017). Historical greenhouse gas concentrations for climate modeling (CMIP6). *Geoscientific Model Development*, *10*(5), 2057–2116. https://doi.org/10.5194/gmd-10-2057-2017

Moch, J. M., Dovrou, E., Mickley, L. J., Keutsch, F. N., Liu, Z., Wang, Y., et al. (2020). Global importance of hydroxymethanesulfonate in ambient particulate matter: Implications for air quality. *Journal of Geophysical Research: Atmospheres*, *125*, e2020JD032706. https://doi.org/10.1029/2020JD032706

Ordóñez, C., Lamarque, J.-F., Tilmes, S., Kinnison, D. E., Atlas, E. L., Blake, D. R., et al. (2012). Bromine and iodine chemistry in a global chemistry-climate model: Description and evaluation of very short-lived oceanic sources. *Atmospheric Chemistry and Physics*, *12*(3), 1423–1447. https://doi.org/10.5194/acp-12-1423-2012

Parrella, J. P., Jacob, D. J., Liang, Q., Zhang, Y., Mickley, L. J., Miller, B., et al. (2012). Tropospheric bromine chemistry: Implications for present and pre-industrial ozone and mercury. *Atmospheric Chemistry and Physics*, *12*(15), 6723–6740. https://doi.org/10.5194/acp-12-6723-2012

Röthlisberger, R. (2003). Limited dechlorination of sea-salt aerosols during the last glacial period: Evidence from the European Project for Ice Coring in Antarctica (EPICA) Dome C ice core. *Journal of Geophysical Research*, *108*(D16), 3645. https://doi.org/10.1029/2003JD003604

Sherwen, T., Evans, M. J., Carpenter, L. J., Schmidt, J. A., & Mickley, L. J. (2017). Halogen chemistry reduces tropospheric O_3 radiative forcing. *Atmospheric Chemistry and Physics*, *17*(2), 1557–1569. https://doi.org/10.5194/acp-17-1557-2017

Sigl, M., McConnell, J. R., Layman, L., Maselli, O., McGwire, K., Pasteris, D., et al. (2013). A new bipolar ice core record of volcanism from WAIS Divide and NEEM and implications for climate forcing of the last 2000 years. *Journal of Geophysical Research*, *118*, 1151–1169. https://doi.org/10.1029/2012JD018603

Travis, K. R., Jacob, D. J., Fisher, J. A., Kim, P. S., Marais, E. A., Zhu, L., et al. (2016). Why do models overestimate surface ozone in the Southeastern United States? *Atmospheric Chemistry and Physics*, *16*(21), 13561–13577. https://doi.org/10.5194/acp-16-13561-2016

US EPA (2016). *2014 national emissions inventory (NEI) data*. Retrieved from https://www.epa.gov/air-emissions-inventories/2014-national-emissions-inventory-nei-data

van Donkelaar, A., Martin, R. V., Leaitch, W. R., Macdonald, A. M., Walker, T. W., Streets, D. G., et al. (2008). Analysis of aircraft and satellite measurements from the Intercontinental Chemical Transport Experiment (INTEX-B) to quantify long-range transport of East Asian sulfur to Canada. *Atmospheric Chemistry and Physics*, *8*, 2999–3014. https://doi.org/10.5194/acp-8-2999-2008

van Marle, M. J. E., Kloster, S., Magi, B. I., Marlon, J. R., Daniau, A.-L., Field, R. D., et al. (2017). Historic global biomass burning emissions for CMIP6 (BB4CMIP) based on merging satellite observations with proxies and fire models (1750–2015). *Geoscientific Model Development*, *10*(9), 3329–3357. https://doi.org/10.5194/gmd-10-3329-2017

Wang, Q., Jacob, D. J., Fisher, J. A., Mao, J., Leibensperger, E. M., Carouge, C. C., et al. (2011). Sources of carbonaceous aerosols and deposited black carbon in the Arctic in winter-spring: Implications for radiative forcing. *Atmospheric Chemistry and Physics*, *11*(23), 12453–12473. https://doi.org/10.5194/acp-11-12453-2011

Wang, Q., Jacob, D. J., Spackman, J. R., Perring, A. E., Schwarz, J. P., Moteki, N., et al. (2014). Global budget and radiative forcing of black carbon aerosol: Constraints from pole-to-pole (HIPPO) observations across the Pacific: Global BC budget and radiative forcing. *Journal of Geophysical Research*, *119*(1), 195–206. https://doi.org/10.1002/2013jd020824

Wang, Y., Jacob, D. J., & Logan, J. A. (1998). Global simulation of tropospheric O_3-NO_x-hydrocarbon chemistry: 1. Model formulation. *Journal of Geophysical Research*, *103*(D9), 10713–10725. https://doi.org/10.1029/98JD00158

Wesely, M. L. (1989). Parameterization of surface resistances to gaseous dry deposition in regional-scale numerical models. *Atmospheric Environment*, *23*(6), 1293–1304. https://doi.org/10.1016/0004-6981(89)90153-4

Zhang, L., Gong, S., Padro, J., & Barrie, L. (2001). A size-segregated particle dry deposition scheme for an atmospheric aerosol module. *Atmospheric Environment*, *35*(3), 549–560. https://doi.org/10.1016/S1352-2310(00)00326-5

Zhu, L., Jacob, D. J., Eastham, S. D., Sulprizio, M. P., Wang, X., Sherwen, T., et al. (2019). Effect of sea salt aerosol on tropospheric bromine chemistry. *Atmospheric Chemistry and Physics*, *19*(9), 6497–6507. https://doi.org/10.5194/acp-19-6497-2019